Vehicle–pedestrian collisions: validated models for pedestrian impact and projection

D P. Wood[1], **C K Simms**[2]* and **D G Walsh**[3]
[1]Denis Wood Associates, Dublin, Eire
[2]Department of Mechanical Engineering, Trinity College, Dublin, Eire
[3]J H Burgoyne and Partners LLP, Stevenage, UK

The manuscript was received on 21 June 2004 and was accepted after revision for publication on 30 September 2004.

DOI: 10.1243/095440705X6703

Abstract: The most important factor in pedestrian injuries from vehicle collisions is the impact velocity. In cases where the impact configuration can be ascertained, the most common method now used to determine vehicle speed involves the pedestrian projection distance. The more traditional method of using tyre brake marks is losing applicability as ABS braking systems become more common. The two most common impact configurations are wrap projection and forward projection, these being determined by the vehicle/pedestrian geometry and the initial conditions of the impact. In this paper, two models are presented for pedestrian forward and wrap projection impacts. These models are predicated on separating the total projection distance into the individual projection distances occurring during three principal phases of the collision. The models are novel as they use a rigid single-segment body representation of the pedestrian, include explicit modelling of the impact phase, and also allow for uncertainty in the input parameters. Published data are used to provide distributions for the input variables such as pedestrian and vehicle masses, etc. The model predictions of impact speed from overall projection distance are validated by comparison with real-world accident data.

Keywords: pedestrian collisions, projection distance, impact speed, coefficient of retardation

1 INTRODUCTION

Pedestrian injuries and fatalities from vehicle collisions vary with environment, urban or rural and country. While the age and state of health of the pedestrian, the nature of the impact, and the vehicle design all affect the injury outcome, the prime factor in injury/fatality risk is the vehicle speed [**1**–**2**]. This has implications for legislators in designing speed limits for built-up areas, for safety engineers in reducing vehicle aggressivity, and for biomechanics research into injury causation, and legal implications in determining driver culpability and pedestrian compensation following an accident.

The use of the pedestrian projection distance as a measure of pre-impact vehicle speed is increasingly important. The methods can be categorized as empirical [**3**–**5**], deterministic [**6**–**8**], or statistical [**9**–**11**]. Empirical models do not contribute towards understanding the physical nature of the impact and projection process. Deterministic models derive from fundamental equations, while statistical models additionally allow for variability of the collision circumstances. Thus, empirical and statistical models provide a range of predicted vehicle speeds for a given projection distance, while deterministic models provide a single estimate of vehicle speed without confidence bounds.

In reality, not all of the factors relating the projection distance to impact speed can be determined, and some of the collision mechanisms are not fully understood (e.g. continued vehicle/pedestrian interaction and the pedestrian/ground contact mechanism), so a degree of uncertainty is inevitable. In this paper, simple analytical statistical models for forward and wrap pedestrian impacts are presented. Unlike other models that concentrate on the particle representation of the pedestrian and on the projection phase of pedestrian–vehicle collisions, these single-segment models explicitly model both the impact and projection phases and account for uncertainty in the input parameter distributions.

* *Corresponding author: Centre for Bioengineering, Department of Mechanical Engineering, Trinity College, Dublin, Eire. email: csimms@tcd.ie*

2 PEDESTRIAN IMPACT AND PROJECTION: KINEMATIC OBSERVATIONS

The majority of pedestrian collisions occur with the fronts of vehicles and are classified into four distinct impact configurations [**12**, **13**]:

(a) wrap projection;
(b) forward projection;
(c) fender vault;
(d) roof vault.

Pedestrian/vehicle geometry and respective velocities at the time of impact determine the specific configuration. Full engagement of the pedestrian with the vehicle is defined as occurring when the vehicle and pedestrian attain a substantially equal post-impact velocity prior to restitution and separation. This may not occur if there is a significant pre-impact transverse velocity of the pedestrian or corner impact. Most frontal pedestrian collisions involve full engagement with the vehicle [**14**] and are classified as either 'forward' or 'wrap' projection collisions. In some instances, categorization may be difficult as aspects of two or more of the above classifications may be fulfilled. In these circumstances, accident reconstruction must proceed with additional caution.

Forward projection occurs when a high-fronted vehicle strikes a pedestrian, or a passenger vehicle strikes a child pedestrian. Here, the pedestrian's centre of gravity is below the leading edge of the bonnet and above bumper level. The impact projects the pedestrian horizontally, with the pedestrian's feet mostly in contact with the ground, although the shoulders and head may rotate about the bonnet edge and impact its upper surface. This is followed by the pedestrian fall-over phase and subsequent ground impacts with slide, roll, and bounce to rest.

Wrap projection occurs when the centre of gravity of the pedestrian is higher than the leading edge of the bonnet, resulting in rotation (wrap) of the pedestrian over the bonnet. The front of the vehicle strikes the legs and thigh/pelvic areas (primary impact) and this is followed by secondary (head and/or shoulder) impact with the vehicle. After this, continued interaction with the vehicle or a flight phase may occur, or a combination of both, followed by ground impact(s) and slide, roll, and bounce to rest.

Some frontal collisions are with the corner of the vehicle where the pedestrian is deflected to one side without secondary impact of the upper body with the vehicle front. Alternatively, the transverse velocity of the pedestrian at impact may be sufficient to prevent head contact as the body rotates sideways off the bonnet, and these situations are known as fender vault. The models presented here do not apply to fender vault.

In each case there are many confounding factors including: vehicle geometry, impact duration, continued pedestrian/vehicle interaction and restitution, pre-impact pedestrian transverse velocity, vehicle braking, the extent of contact between the pedestrian's feet and the ground during fall-over, and the nature of the bounce–roll–slide to rest of the pedestrian.

3 MODELS

The models presented here represent the pedestrian as a rigid, single-segment body.

3.1 Forward projection

The forward projection model considers pedestrian movement during three distinct phases:

(a) impact;
(b) fall-over;
(c) slide/roll/bounce to rest.

The total projection distance of the pedestrian is the sum of the distance travelled in each individual phase (see Fig. 1)

$$S_{\text{total}} = S_{\text{impact}} + S_{\text{fall-over}} + S_{\text{slide/roll/bounce}} \tag{1}$$

3.1.1 Impact

During the impact phase of the collision, there is a momentum transfer between the vehicle (mass M_{v}) and the pedestrian (mass M_{p}). The pre-impact vehicle speed is V_{col}. As a result of momentum conservation and restitution effects, e, the post-impact horizontal projection velocity, V_{proj}, of the pedestrian centre of gravity (CG) is

$$V_{\text{proj}} = \frac{M_{\text{v}}}{M_{\text{v}} + M_{\text{p}}}[1 + e]V_{\text{col}} \tag{2}$$

The momentum transfer occurs over a time interval equal to the impact duration, t_{impact}. The distance travelled by the pedestrian during this time is approximated as

$$S_{\text{impact}} = V_{\text{proj}}\, t_{\text{impact}} \tag{3}$$

At the end of the impact stage the momentum transfer is complete and it is assumed that no further interaction between the vehicle and pedestrian occurs.

d000001504 08-12-04 13:30:44 Rev 14.05
The Charlesworth Group, Huddersfield 01484 517077

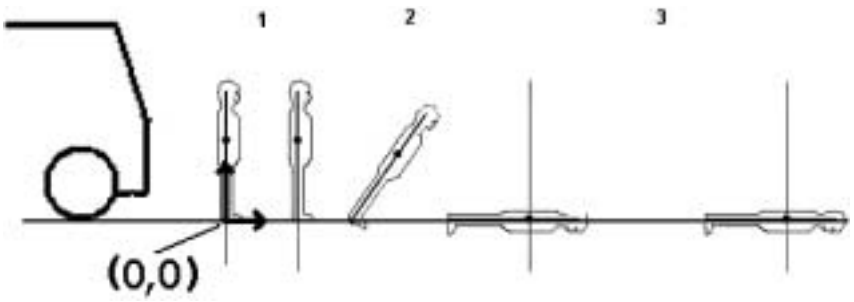

Fig. 1 Schematic of the forward projection sequence, showing the system origin

Owing to the geometry of impact (the pedestrian CG lies below the upper edge of the vehicle front, e.g. the leading edge of the bonnet of cars) there is no rotational component to pedestrian movement and the pedestrian is modelled as maintaining an upright orientation during this phase.

3.1.2 *Fall-over*

This phase follows directly from the impact phase described above. The pedestrian CG now has a horizontal velocity, V_{proj}, and it is assumed that his/her feet remain in contact with the ground. This results in frictional load acting to retard the base/feet of the pedestrian, causing the pedestrian to rotate. As fall-over commences, gravitational effects further contribute to rotation of the pedestrian. This is modelled using a single rigid segment to represent the initially vertical pedestrian (see Fig. 1). The distance from the centre of gravity to the ground is h, the ground reaction force is R, and the accompanying friction force is μR. The motion is considered to be planar and the three equations of motion of the CG of the pedestrian segment with mass M_{p} and radius of gyration k can then be written as

$$M_{\text{p}}\ddot{x} = -\mu R \tag{4}$$

$$M_{\text{p}}\ddot{y} = M_{\text{p}}g - R \tag{5}$$

$$M_{\text{p}}k^2\ddot{\phi} = hR\sin(\phi) + \mu Rh\cos(\phi) \tag{6}$$

The following additional constraint is imposed: the base of the segment (representing the feet) remains in contact with the ground during fall-over, which is expressed as

$$\ddot{y} = h(\dot{\phi})^2\cos(\phi) + h\ddot{\phi}\sin(\phi) \tag{7}$$

The constraint in equation (7) effectively couples the vertical and rotational motion, and the equations can be rearranged to contain functions of the variables x and ϕ only

$$\begin{bmatrix} 1/\mu & -h\sin(\theta) \\ 0 & -h\left(\sin(\phi) - \dfrac{k^2}{h(\sin(\phi) + \mu\cos(\phi))}\right) \end{bmatrix} \begin{pmatrix} \ddot{x} \\ \ddot{\phi} \end{pmatrix} = \begin{bmatrix} h(\dot{\phi})^2\cos(\phi) - g \\ (\dot{\phi})^2\cos(\phi) - g \end{bmatrix} \tag{8}$$

These coupled second-order differential equations were integrated using a Runge–Kutta integration scheme, with the following initial conditions

$$\begin{pmatrix} \dot{x} \\ x \\ \dot{\phi} \\ \phi \end{pmatrix}_{t=0} = \begin{pmatrix} V_{\text{proj}} \\ S_{\text{impact}} \\ 0 \\ 0 \end{pmatrix} \tag{9}$$

The integration is terminated when the fall-over angle, ϕ, has reached 90° ($t = t_{\phi=90}$), and the horizontal distance travelled by the pedestrian during this phase, $S_{\text{fall-over}}$, is

$$S_{\text{fall-over}} = (x)_{t(\phi=90)} - S_{\text{impact}} \tag{10}$$

3.1.3 *Slide/roll/bounce to rest*

At the end of the fall-over phase, the segment CG strikes the ground with a vertical velocity

$$V_{\text{v}} = h(\dot{\phi})_{t(\phi=90)} \tag{11}$$

This vertical impact results of a loss in horizontal momentum, and, for the final phase of the pedestrian segment motion, the initial horizontal velocity of the CG is

$$V_{\text{proj f}} = (\dot{x})_{t(\phi=90)} - \mu(V_{\text{v}})_{t(\phi=90)} \tag{12}$$

The deceleration of the segment under the action of friction during slide/roll/bounce to rest can be modelled using the equation of uniform acceleration,

d000001504 08-12-04 13:30:44 Rev 14.05
The Charlesworth Group, Huddersfield 01484 517077

and the horizontal distance travelled, $S_{\text{slide/roll/bounce}}$, is

$$S_{\text{slide/roll/bounce}} = \frac{V_{\text{proj f}}^2}{2\mu g} \tag{13}$$

It should be noted that μ is the coefficient of effective retardation (rather than the formal coefficient of friction) and the same μ is used during fall-over and slide.

3.2 Wrap projection

The wrap model presented in this paper considers pedestrian movement during the three phases of vehicle/pedestrian impact, including wrap over the bonnet and restitution, flight, and slide/roll/bounce to rest. The total projection distance of the pedestrian is the sum of the distance travelled in each individual phase (see Fig. 2)

$$S_{\text{total}} = S_{\text{impact}} + S_{\text{flight}} + S_{\text{slide/roll/bounce}} \tag{14}$$

3.2.1 *Impact*

Following primary impact with the front of the vehicle, rotation of the pedestrian onto the bonnet with a secondary impact occurs, generally between the bonnet/windscreen and the head/shoulders. Separation of the pedestrian and the vehicle after secondary impact occurs mainly owing to a combination of vehicle braking and the pedestrian's vertical and lateral motion. At low/moderate impact speeds, the pedestrian may drop back onto the bonnet following this secondary impact and even remain in contact with the leading edge of the bonnet during rotation to head/shoulder contact. Following separation, the flight and slide/roll/bounce to rest phases begin.

Wood [**15**–**16**] has previously derived a single-segment pedestrian projection model which has been validated using real-life accidents involving a variety of car types and shapes reconstructed as part of the KOB project (D. Cesari, 1989, personal communication). This validation showed that the single-segment model (SSM) satisfactorily predicted the mean time to secondary impact, the mean location of the secondary impact (wrap-around ratio), the mean velocity of the pedestrian's head at secondary impact, as well as the mean collision speed to projection distance relationship [**15**–**17**]. Wood's SSM used momentum conservation to derive the angular and linear velocities of a rigid pedestrian segment following primary and secondary impact with the vehicle front and bonnet/windscreen respectively. These closed-form equations yielded pedestrian kinematics as a function of impact speed, mass (pedestrian and vehicle), and basic geometry (radius of gyration, impact locations, and vehicle profile).

Primary impact. Owing to the horizontal momentum transfer from the vehicle to the pedestrian CG, and before restitution effects, the common post-impact velocity of the vehicle is

$$V_{\text{cp}} = \left[\frac{M_{\text{v}}}{M_{\text{v}} + M_{\text{p}}}\right] V_{\text{col}} \tag{15}$$

Modelling of the SSM was carried out for a representative range of pedestrian heights and car profiles for the full range of vehicle braking conditions during primary and secondary impacts. Regression analysis shows that the distance travelled by the pedestrian between primary and secondary impact can be statistically represented as

$$S_{\text{impact}} = 0.887^{(1 \pm 1.3t)} V_{\text{cp}}^{0.1665} \tag{16}$$

where t is the normally distributed random variable (mean = zero, standard deviation = 1). This regression includes the displacement of the pedestrian during primary impact [**13**].

Secondary impact. Figure 3 shows the secondary impact between the pedestrian's head/shoulders and the vehicle. Further regression analysis of Wood's SSM shows that, after secondary impact of the pedestrian with the car, and when vehicle braking occurs (μ_{braking} varying from 0 to 1.0g), the post-impact horizontal velocity of the pedestrian before restitution, V_{h}, can be expressed as

$$V_{\text{h}} = 0.649^{(1 \pm 0.13t)} V_{\text{cp}}^{0.1665} \tag{17}$$

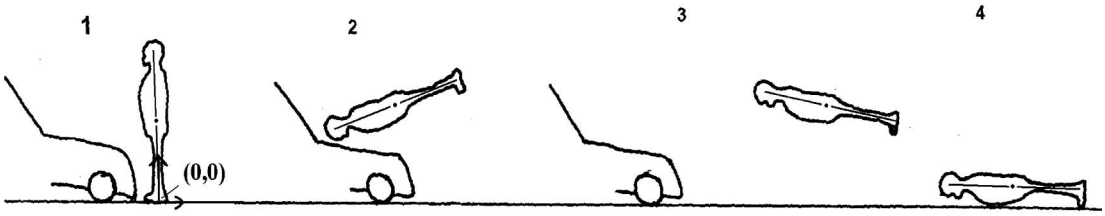

Fig. 2 Schematic of the wrap projection sequence, showing the system origin

d000001504 08-12-04 13:30:44 Rev 14.05
The Charlesworth Group, Huddersfield 01484 517077

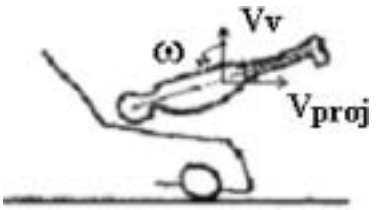

Fig. 3 Pedestrian/vehicle interaction during wrap projection

where again t is a normally distributed random variable. (The upper bound for V_h was set equal to V_{cp}.) When there is no braking during the vehicle–pedestrian impact phase, then

$$V_h = V_{cp} \tag{18}$$

Using the KOB report (D. Cesari, 1989, personal communication), braking is modelled as occurring in 85 per cent of cases. Accounting for restitution effects, the final horizontal velocity of the pedestrian, V_{proj}, is

$$V_{proj} = (1 + e)V_h \tag{19}$$

The eccentric nature of the primary and secondary impacts with the vehicle front imparts an angular velocity to the pedestrian segment, and, following secondary impact with the bonnet/windscreen, regression of Wood's SSM shows that the resulting mean vertical velocity of the pedestrian CG, $V_{v\,mean}$, can be represented as

$$\frac{V_{v\,mean}}{V_{cp}} = 0.0675 \times [V_{cp} - 6]^{0.369} \tag{20}$$

while the standard deviation of vertical velocity, V_v, is $V_{v\,mean}/3$. For individual collisions the vertical velocity is represented as

$$V_v = V_{v\,mean} \pm \frac{V_{v\,mean}}{3} t \tag{21}$$

where t is a normally distributed variable.

The cut-off limit of 6 m/s for V_{cp} in equation (20) is the maximum combined vehicle and pedestrian velocity below which detailed SSM modelling showed that gravitational effects cause the pedestrian to drop back onto the bonnet prior to separation, and the vertical component of flight velocity is therefore zero. At high impact speeds, the model has the capability to model roof vault cases, where the higher pedestrian vertical velocity from the increased angular momentum after primary impact yields increased vertical and rotational velocities after secondary impact.

The orientation change of the pedestrian between primary and secondary impacts with the vehicle can be represented as

$$\theta_{deg} = 69^{(1 \pm 0.0143t)} \times V_{cp}^{0.164} \tag{22}$$

and Fig. 3 shows that this increases the height of the pedestrian CG by

$$d_{CG} = 0.63 \times \text{height} - 0.15 + (0.37 \times \text{height} + 0.1) \times \sin(\theta - 90) \tag{23}$$

3.2.2 *Flight*

After head/shoulder (secondary) impact, the flight phase is assumed to commence. The time taken for ground contact to occur is

$$t_{flight} = \frac{V_v + (V_v^2 + 2gd_{CG})^{1/2}}{g} \tag{24}$$

and the horizontal distance travelled by the pedestrian during the flight phase is

$$S_{flight} = [V_{proj} \times t_{flight}] \tag{25}$$

3.2.3 *Slide/roll/bounce to rest*

At the end of the flight phase, the pedestrian CG strikes the ground with a vertical velocity

$$V_{vf} = (V_v^2 + 2gd_{CG})^{1/2} \tag{26}$$

The vertical impact results in a loss of horizontal momentum, and, for the final phase of motion, the initial horizontal velocity of the CG is

$$V_{proj\,f} = V_{proj} - \mu \times V_{vf} \tag{27}$$

The deceleration due to friction during slide/roll/bounce to rest is modelled using the equation of uniform acceleration, and the horizontal distance travelled, $S_{slide/roll/bounce}$, is

$$S_{slide/roll/bounce} = \frac{V_{proj\,f}^2}{2\mu g} \tag{28}$$

3.3 Input data for the models

Equations (1) and (14) detail the relationship between projection distance and impact velocity for forward and wrap projection impacts respectively. However, the application of these equations requires knowledge of the parameters M_p, M_v, μ, h, k, and e (again, it should be noted that μ is the coefficient of retardation rather than the coefficient of Coulomb friction, as the slide/roll/bounce interaction is complex and not fully understood). It is generally not possible to

d000001504 08-12-04 13:30:44 Rev 14.05
The Charlesworth Group, Huddersfield 01484 517077

ascertain all of this information for a given accident, and so it is appropriate to consider the statistical distribution of these parameters. All of the input parameters have been approximated using standard statistical distributions (normal, log normal, uniform, etc.) based on values obtained from the published literature. The coefficient of restitution was estimated from experimental tests using dummies by Lucchini and Weissner [**18**], while the impact duration times are derived from cadaver tests by Aldman [**19**]. Further details of all the distributions used in these models are presented in Appendix 2. While it is recognized that the biofidelity of current crash dummies is limited, there is at present no alternative means to estimate the distributions of restitution in vehicle pedestrian collisions.

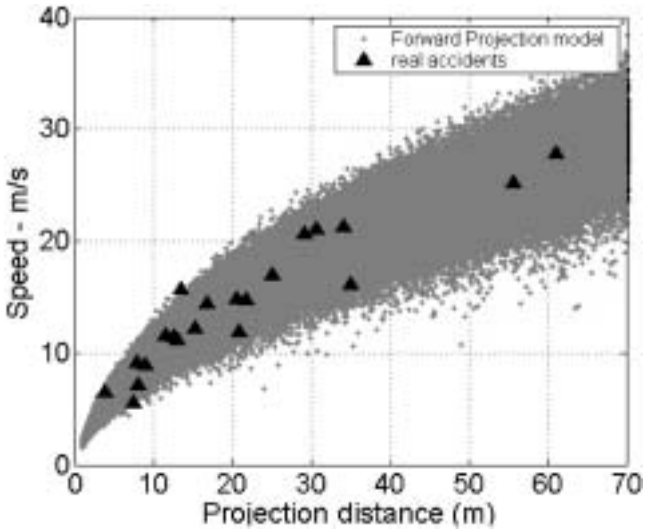

Fig. 4 Real accident data and scatterplot predictions of collision speed versus projection distance in forward projection ($N = 21$)

4 RESULTS

There are two relevant aspects to the validation of these models: the accuracy of the mean prediction of velocity, and the degree of scatter about the mean at a given projection distance compared with real-world data. Real world data on projection distance versus impact speed are derived from accident cases where projection distance was measured and an alternative means of speed estimation was available.

4.1 Validation for the forward projection model

The Monte Carlo method was used to account for the statistical uncertainty of the input parameters for the models. The resulting scatter of velocity prediction data as a function of projection distance was compared with the available real accident data for real-life adult forward projection cases [**20**, **21**] (see Fig. 4).

The models clearly encompass the real accident data very well. There are insufficient test data to characterize the standard deviation of test velocities at each projection distance, but it can be seen that the variability in the test data is well matched by the cloud of model predictions. Furthermore, linear regression of the scatterplot data of the form

$$V_{\text{col}} = A\sqrt{S} + B \tag{29}$$

yielded very high correlation coefficients (see Table 1). Using the mean regression, the predicted velocity was evaluated at each of the experimental projection distances. The difference between the model and real accident velocity at each projection distance was defined as

$$V_{\text{diff}} = V_{\text{real}} - V_{\text{model}} \tag{30}$$

The distribution of V_{diff} approximates well to a normal distribution and the paired t test (H_0: mean $V_{\text{diff}} = 0$; H_1: mean difference $\neq 0$) showed no statistically significant difference at the 95 per cent confidence level compared with the real-life data ($t = -0.28$, $p = 0.784$). Figure 5 shows that the prediction error is independent of collision speed. Linear regression confirms the absence of correlation, $r^2 = 0.08$. It is concluded that the model provides a good prediction of both the mean and the scatter in collision velocity for forward projection cases as a function of projection distance.

Table 1 Global forward projection and wrap model limits

	Forward projection (V_{col} (m/s) $= A\sqrt{S\text{ (m)}} + B$)			Wrap projection (V_{col} (m/s) $= C \times [S\text{ (m)} - S_{\text{o}}]^D$)			
Confidence level for velocity prediction	A	B	R	S_{o}	C	D	R
Lower 0.1 percentile	2.5	−1.2	0.99	1.9	2.3	0.51	0.99
Mean	3.7	−1.5	0.99	1.6	4.0	0.47	0.99
Upper 0.1 percentile	4.6	−1.0	0.99	1.2	5.3	0.46	0.99

d000001504 08-12-04 13:30:44 Rev 14.05
The Charlesworth Group, Huddersfield 01484 517077

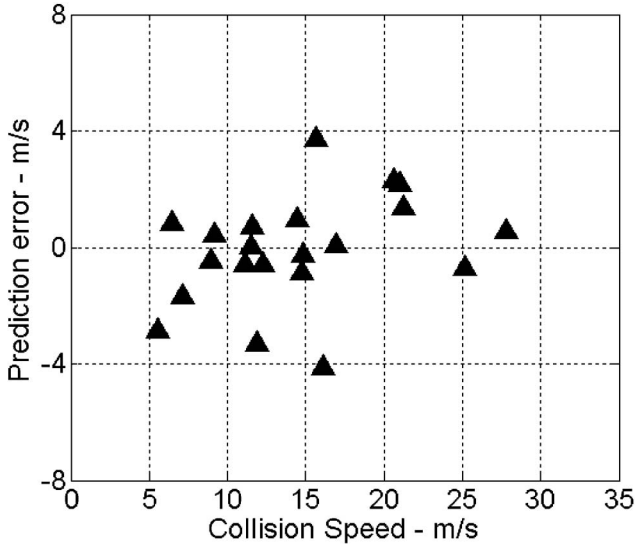

Fig. 5 Prediction error versus real-world collision speed for forward projection

4.2 Validation for the wrap projection model

As with forward projection, the wrap projection model was run using the Monte Carlo method to account for statistical uncertainty in the input parameters. The resulting scatter of data was compared with the available data for real accident cases [**21**–**26**] (see Fig. 6). There are far more real-world data available ($N = 185$) for this impact configuration, allowing a more comprehensive comparison of the mean and variability of the accident data compared with the model predictions.

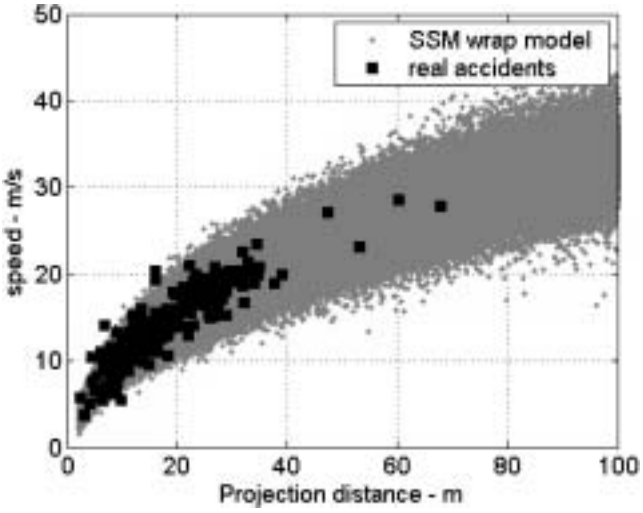

Fig. 6 Real accident data and scatterplot predictions of collision speed versus projection distance in wrap projection ($N = 185$)

For the wrap model, the linear relationship between $S^{1/2}$ and V_{col} does not hold at very low speeds, and a power regression of the scatterplot data of the form

$$V_{\text{col}} = C \times [S - S_{\text{o}}]^D \tag{31}$$

is more appropriate. The value of S_{o} was chosen to maximize the regression coefficient, and the model parameters are given in Table 1. Using the mean regression, the predicted velocity was evaluated at each of the experimental projection distances. The difference between the model and real accident velocity at each projection distance was again defined using equation (30), and analysis showed these to approximate well to a normal distribution. The paired t test (H_0: mean $V_{\text{diff}} = 0$, H_1: mean difference $\neq 0$) showed no statistically significant difference at the 95 per cent confidence level ($t = -0.61$, $p = 0.55$).

Figure 7 shows the difference between the real-life and predicted velocities as a function of real accident impact velocity. The data appear to show a weak biasing effect in which the model overpredicts collision speed at low velocities and underpredicts at high velocities. However, owing to the large size of the real accident dataset, $N = 185$, it is possible to evaluate this by comparing the model and the real accident data for specific projection distance bands. The accident data were divided into 20 equal $\sqrt{s}$ bins, and Fig. 8 shows the mean and ± 1 standard deviation of collision velocity in each bin as a function of throw distance. At higher throw distances, where there was only one accident point in each bin, the standard deviations for the test data could not be included. Figure 8 also shows the corresponding data from the model predictions. It is clear that there is a very good

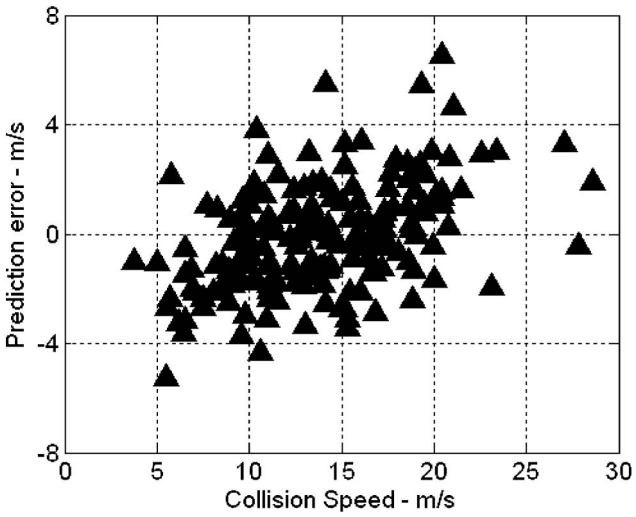

Fig. 7 Prediction error versus collision speed for wrap projection

d000001504 08-12-04 13:30:44 Rev 14.05
The Charlesworth Group, Huddersfield 01484 517077

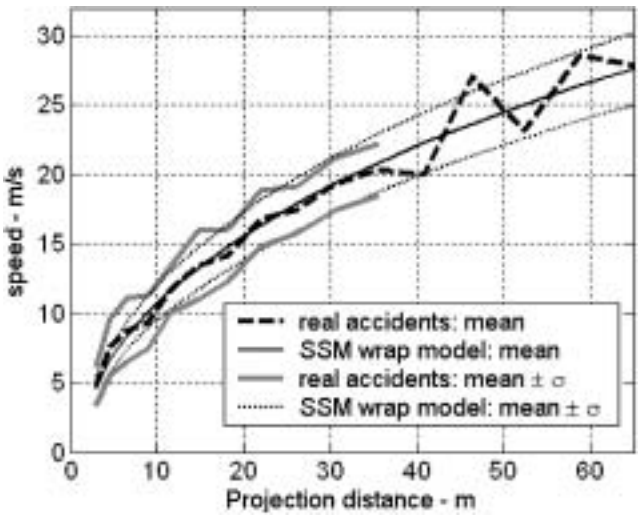

Fig. 8 Comparison of the mean and standard deviation of the SSM wrap model and the real accident data

correspondence for both the mean and the variability of the model data compared with the real-world accident data. Furthermore, the apparent biasing effect seen in Fig. 7 is not present. It is therefore concluded that the model provides a good method for predicting collision velocity from throw distance for wrap projection cases.

Very recently, Otte [**27**] has published data on over 300 wrap projection real accidents recorded in Germany between 1985 and 2001. Figure 9 shows a comparison between all of the previous wrap projection real accident cases (used in the validation in this paper) and the new data presented by Otte.

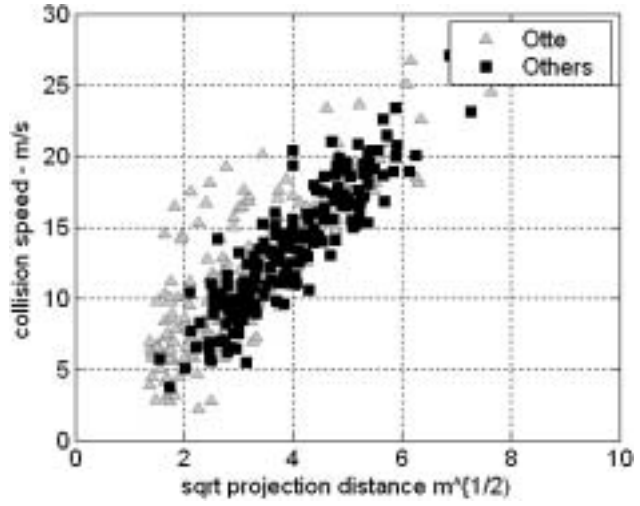

Fig. 9 Comparison of reported real-world wrap projection cases: Otte [**27**] and other researchers [**21**–**26**]

While there is good agreement between these two datasets for both mid and high projection distances, at low projection distances these two datasets show distinct differences. Otte reported all of these accidents as frontal, with pedestrian contact occurring not less than 20 cm from each bonnet edge. However, inspection shows cases with impact speeds up to 60 km/h where the projection distance is less than 4 m. This indicates strongly that full engagement of the pedestrian with the vehicle front did not take place. As previously mentioned, this would occur if the pedestrian had a significant transverse velocity at impact, resulting in rotation off the side of the vehicle after primary impact. These cases are more correctly classified as fender vault and should not be treated as wrap projection cases.

5 DISCUSSION

5.1 Previous models

There are many published models for speed prediction from projection distance, of which recent papers by Toor and Araszewski [**5**] and Han and Brach [**11**] provide a comprehensive review. In this paper, only those previous models that best characterize their respective approaches are discussed.

The mean prediction from most models compares favourably with a mean regression line fitted to a set of experimental data, and this has generally been the method used to 'validate' a new model. However, there is considerable scatter of the real-world data about the mean, and any valid model must also reflect this uncertainty.

The small sample size ($n < 21$) of real-world data for forward projection cases precludes determination of confidence limits for collision speed at a particular throw distance. For wrap projection cases, the larger sample size ($N = 185$) makes this more feasible, and Evans and Smith [**28**] have performed a least-squares linear regression of V_{col} against $s^{1/2}$. They present their best fit line together with the 95 per cent limits, which are shown here in Fig. 10. Evans and Smith used only Hill and Dettinger data [**22**, **23**] on the basis that this was more up to date and displayed less scatter than older data. However, this approach can be flawed, as is seen by comparison with even newer data from Field [**21**] (see Fig. 10). The 95 per cent confidence limits for the mean and even the absolute minimum curve predicted by Evans and Smith based on the Hill and Dettinger data alone fails to encompass the scatter in the Field data. This highlights the pitfalls of an empirical approach—the

d000001504 08-12-04 13:30:44 Rev 14.05
The Charlesworth Group, Huddersfield 01484 517077

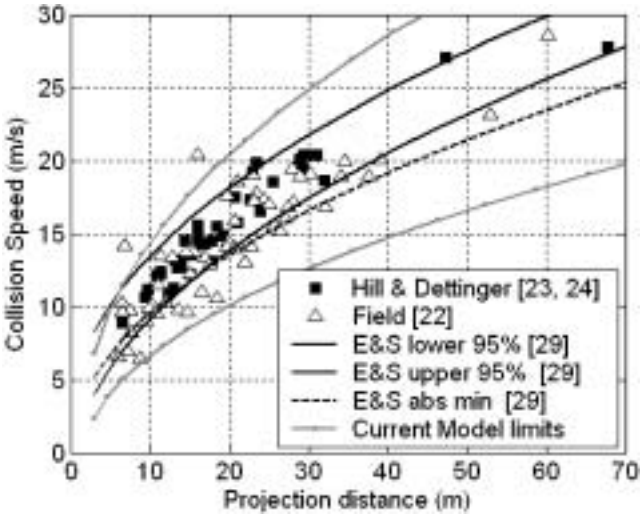

Fig. 10 Comparison of real accident data for wrap projection with previous work

predictions are only correct for the real accident cases considered. More recently, Toor and Araszewski [**5**] have derived empirical models based on power law regressions, and, again, the 95 per cent limits for the mean are given. However, for both wrap and forward projection cases, even the test data used to derive the Toor–Araszewski models contain several cases lying outside the 95 per cent limits presented, thus making those confidence limits not very robust. The Toor–Araszewski model mean and lower 95 per cent limits for wrap projection are shown in Fig. 11. Similarly, the Toor–Araszewski model mean and lower 95 per cent limits for forward projection are shown in Fig. 12. It can be seen that the Toor–Araszewski mean and minimum predictions are quite good,

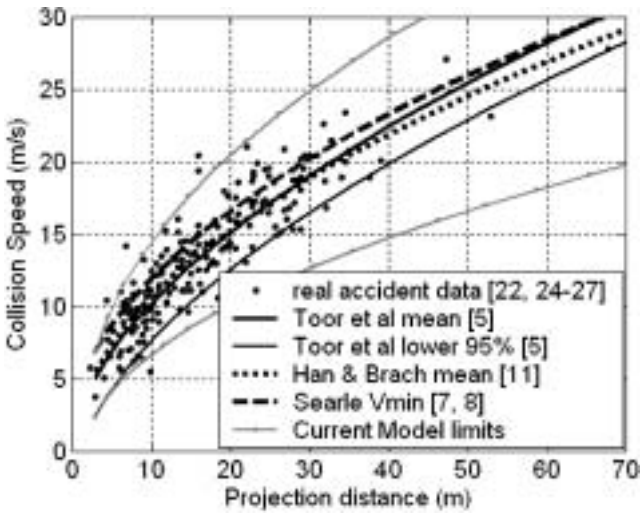

Fig. 11 Comparison of real accident data for wrap projection with previous work

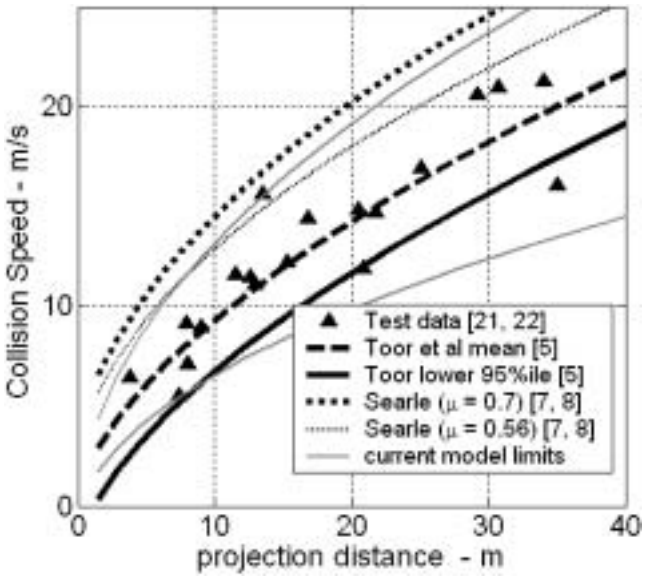

Fig. 12 Comparison of real accident data for forward projection with previous work

although the small sample size makes the robustness of the minimum prediction difficult to assess.

5.2 Analytical models

Searle's particle model [**7**, **8**] in which launch angle, coefficient of retardation, and horizontal momentum loss due to vertical ground impacts are considered, is the most 'physical' of the early models. The impact phase is not explicitly modelled. Searle accounted for pedestrian/vehicle momentum interchange (by using a 20 per cent correction factor for adults) but did not distinguish between different impact configurations. However, Searle's model is effectively a slide model when the projection angle is set to zero (see Fig. 12). In that case, Searle's prediction provides a velocity estimate that is higher than the test data. Searle assumed a retardation coefficient $\mu = 0.7$, and this is part of the reason why his collision speed estimates are too high, but, even when a more realistic value is used ($\mu = 0.56$), the curve is still too high (see Fig. 12). For wrap projection cases, Searle minimized his projection distance equation with respect to the launch angle (which is generally unknown) to arrive at a minimum velocity prediction (see Fig. 11). This minimum prediction is again too high, partly because of the high coefficient of retardation he used, but also because of the constant momentum interchange factor he employed.

In addition, there is further difficulty with Searle's model—the projection distance used is the total horizontal displacement of the pedestrian from impact to rest. In reality this distance includes the distance

d000001504 08-12-04 13:30:44 Rev 14.05
The Charlesworth Group, Huddersfield 01484 517077

travelled by the pedestrian during the contact period with the vehicle, which is ignored by Searle. In this respect, he has not fully considered the physics of the collision.

More recently, Han and Brach [**11**] developed a semi-analytic projection distance model in which they include an impact phase distinct from the projection phase. However, lacking a means of calculating the distance travelled during the impact phase, these authors used an empirically tuned arbitrary function relating travel distance to impact velocity. Also, an arbitrary distribution was used for projection angle.

5.3 Complex multi-body models

Finite element and multi-body techniques are capable of detailed modelling of vehicle and human body characteristics as well as the complex loading patterns that occur during an impact. In 1983, van Wijk *et al.* [**6**] used multi-body models with up to 15 segments to predict whole body kinematics and head impact velocities which correlated well with dummy experiments. Since then, the finite element model of Hardy *et al.* [**29**] and Yang and Lovsund's multi-body model (ca 50 segments) [**30**] have both been successfully used to predict detailed interactions between pedestrians and vehicles in cases where the collision configuration is well defined [**2**, **31**, **32**]. Moreover, these researchers have used known initial conditions (including vehicle speed) to analyse the injury potential of the vehicle/pedestrian interaction. Even in these cases, certain assumptions regarding retardation coefficients and vehicle dive angle, pedestrian orientation, etc., were necessary. These deterministic models do not incorporate the uncertainty in the input parameters that is inevitably present when reconstructing real-life accidents. The main application for deterministic models has therefore been in parameter studies where the influence of vehicle speed, front-end geometry and stiffness, etc., can be studied with reference to a baseline case [**33–35**].

Bhalla *et al.* [**36**] used multi-body models of three vehicle types and three pedestrian sizes/masses to show that the relationship between speed and projection distance was significantly affected by vehicle/pedestrian characteristics and pedestrian ground retardation. They concluded that the only way to address this problem is to use deterministic multi-body modelling techniques. However, the same parameters they have shown to be crucial for determining vehicle speed (initial conditions, friction, etc.) are generally not available as input to such models. In fact, the variability due to pedestrian orientation and pre-impact speed and continued pedestrian/vehicle interaction will probably always remain as an uncertainty.

At present it is therefore a better approach to accept the uncertainty associated with each input parameter and observe the effect this has on the resulting velocity prediction. This has been used to good effect by Simms *et al.* [**37**] to arrive at a variety of reconstruction tables for various collision conditions.

6 CONCLUSIONS

The wrap and forward projection models linking vehicle speed to pedestrian projection distance that have been presented in this paper accurately reflect both the mean and the variability about the mean that are evident in the published real-world data. The main advances of these models over existing models are the application of a single-segment body model for the pedestrian, explicit modelling of the impact phase, application of fall-over behaviour in place of flight for forward projection, and the inclusion of the uncertainty of the input parameters that is inevitably present in the reconstruction of all real-world pedestrian accidents.

The Monte Carlo technique applied to these models currently provides the best means to predict not only vehicle speed from pedestrian projection distance for real-world cases but also any desired confidence level for these speed predictions [**37**].

7 FUTURE WORK

The simplified nature of the models presented in this paper means that, in each individual collision simulation, many details are omitted. In the future, if distributions of pedestrian/vehicle initial conditions and vehicle stiffness/geometry parameters can be estimated, the Monte Carlo technique can be applied to complex multi-body or even finite element models to combine the benefits of more detailed modelling with the inevitable uncertainty associated with reconstructing real-life accidents.

REFERENCES

1 **Walz, F. H., Hoefliger, M.** and **Fehlmann, W.** Speed limit reduction from 60 to 50 km/h and pedestrian injuries. Proceedings of 27th Stapp Car Crash

d000001504 08-12-04 13:30:44 Rev 14.05
The Charlesworth Group, Huddersfield 01484 517077

Conference Proceedings with International Research Committee on Biokinetics of Impacts (IRCOBI), 1983, pp. 311–318.
2 **Howard, M., Thomas, A., Koch, W., Watson, J.** and **Hardy, R.** Validation and application of a finite element pedestrian humanoid model for use in pedestrian accident simulations. In Proceedings of IRCOBI Conference, 2000, pp. 101, 119.
3 **Evans, A. K.** and **Smith, R.** Vehicle speed calculation from pedestrian throw distance. *Proc. Instn Mech. Engrs, Part D: J. Automobile Engineering*, 1999, **213**, 441–447.
4 **Rau, H.** and **Otte, D.** Car to pedestrian collisions with high speed impact. *J. Verkehrsunfall und Fahrzeugtechnik*, 2001.
5 **Toor, A.** and **Araszewski, M.** Theoretical vs empirical solutions for vehicle/pedestrian collisions. SAE paper 2003-02-0883, 2003.
6 **Van Wijk, J., Wismans, J., Maltha, J.** and **Wittebrood, L.** MADYMO pedestrian simulations. SAE paper 830060, 1983.
7 **Searle, J. A.** and **Searle, A.** The trajectories of pedestrians, motorcycles, motorcyclists, etc., following a road accident. SAE paper 831622, 1983.
8 **Searle, J. A.** The physics of throw distance in accident reconstruction. SAE paper 930659, 1993.
9 **Wood, D. P.** and **Walsh, D. G.** Pedestrian forward projection impact. *Int. J. Crashworthiness*, 2002, **7**(3), 285–305.
10 **Wood, D. P.** and **Simms, C. K.** A hybrid model for pedestrian impact and projection. *Int. J. Crashworthiness*, 2000, **5**(4), 393–403.
11 **Han, I.** and **Brach, R.** Impact throw model for vehicle–pedestrian collision reconstruction. *Proc. Instn Mech. Engrs, Part D; J. Automobile Engineering*, 2002, **216**, 443–453.
12 **Ravani, B., Broughham, D.** and **Mason, R. T.** Pedestrian post-impact kinematics and injury patterns. SAE paper 811024, 1981.
13 **Eubanks, J. J., Hill, P. F., Casteel, D. A.** and **Solomon, S. S.** In *Pedestrian Accident Reconstruction and Litigation* 1998 (Lawyers and Judges Publishing Company).
14 **Wood, D.** Pedestrian impact, injury and accident causation. In *Automotive Engineering and Litigation* (Eds G. A. Peters and B. J. Peters), 1991, Vol. 4, Ch. 3 (John Wiley).
15 **Wood, D. P.** Impact and movement of pedestrian in frontal collisions with vehicles. *Proc. Instn Mech. Engrs, Part D: J. Automobile Engineering*, 1988, **202**(D2), 101–110.
16 **Wood, D. P.** Application of a pedestrian impact model to the determination of impact speed. SAE paper 910814, 1991.
17 **Wood, D. P.** Application of a rigid body impact model to the pedestrian–car collision. In Proceedings of International IRCOBI Conference, 1988, pp. 241–252.
18 **Lucchini, E.** and **Weissner, D.** Differences between the kinematics and loadings of impacted adults and children results from dummy tests. IRCOBI, 1980.
19 **Aldman, B., Thorngren, L., Bunketorp, O.** and **Romanus, B.** An experimental model for the study of lower leg and knee injuries in car pedestrian impacts. IRCOBI, 1980, pp. 180–193.
20 **Toor, A., Araszewski, M., Johal, R., Overgaard, R.** and **Happer, A.** Revision and validation of vehicle/pedestrian collision analysis method. SAE paper 2002-01-0550, 2002.
21 **Field, J.** Analysis of real world pedestrian/vehicle collisions in the United Kingdom. 6th Conference of Institute of Traffic Accident Investigators, 2003, pp. 129–142.
22 **Hill, G. S.** Calculations of vehicle speed from pedestrian throw. *Impact*, Spring 1994, 18–20.
23 **Dettinger, J.** Methods of improving the reconstruction of pedestrian accidents: development differential, impact factor, longitudinal forward trajectory, position of glass splinters (in German). *J. Verkehrsunfall und Fahrzeugtechnik*, December 1996, 324–330; January 1997, 25–30 (two parts).
24 **Grandel, J., Zeisberger, H.** and **Walz, F. H.** Kinematics and head injuries in vehicle/pedestrian accidents at speeds above 50 kph. In Proceedings of IRCOBI Conference, 1986, pp. 189–204.
25 **Schneider, H.** and **Beier, G.** Experiment and accident: comparison of dummy test results and real pedestrian accidents. SAE paper 741177, 1974.
26 **Steffan, H., Moser, A., Geigl, B.** and **Motomiya, Y.** Validation of the coupled PC-Crash—MADYMO occupant simulation model. SAE paper 2000-01-0471, 2000.
27 **Otte, D.** Use of throw distances of pedestrians and bicyclists as part of a scientific accident reconstruction method. SAE paper 200401-1216, 2004.
28 **Evans, A. K.** and **Smith, R.** Vehicle speed calculation from pedestrian throw distance. *Proc. Instn Mech. Engrs, Part D: J. Automobile Engineering*, 1999, **213**, 441–447.
29 **Hardy, R., Watson, J.** and **Howard, M.** Developments in the simulation of real world car to pedestrian accidents using a pedestrian humanoid finite element model. *Int. J. Crashworthiness*, 2000, **5**(1), 102–117.
30 **Yang, J. K.** and **Lovsund, P.** Development and validation of a human body mathematical model for simulation of car pedestrian collisions. In Proceedings of IRCOBI Conference, 1997, pp. 133–149.
31 **Coley, G., de Lange, R., de Oliviera, P., Neal-Sturgess, C. E.** and **Happee, R.** Pedestrian human body validation using detailed real world accidents. In Proceedings of IRCOBI Conference, 2001, pp. 89–102.
32 **Liu, X.** and **Yang, J.** Development of child pedestrian models and evaluation with accident reconstructions. In Proceedings of IRCOBI Conference, 2001, pp. 103–113.
33 **Liu, X. J., Yang, J. K.** and **Lovsund, P.** A study of influences of vehicle speed and front structure on pedestrian impact responses using mathematical models. *J. Traff. Injury Prev.*, 2002, (3), 31–42.

34 Svoboda, J., Solc, Z. and **Cizek, V.** Analysis of collisions between pedestrian and small car. *Int. J. Crashworthiness*, 2003, **8**(3), 269–276.
35 Silva, M. P. T. and **Ambrosio, J. A. C.** Pedestrian impact and run over using a multi-body simulation tool. *Int. J. Crashworthiness*, 1999, **4**(3), 261–271.
36 Bhalla, K. V., Montazemi, P. and **Crandall, J.** Vehicle impact velocity prediction from pedestrian throw distance: trade-offs between throw formulae, crash simulators, and detailed multi-body modeling. In Proceedings of IRCOBI Conference, Munich, Germany, 2002, pp. 263–276.
37 Simms, C. K., Wood, D. P. and **Walsh, D. G.** Confidence limits for impact speed estimation from pedestrian projection distance. *Int. J. Crashworthiness*, 2004, **9**(2), 219–228.
38 FARS, United States Department of Transport Fatal Accident Reporting System, 1975–2002.
39 Pheasant *Bodyspace—Anthropometry, Ergonomics and Design*, 1986 (Taylor and Francis).
40 Burg, H. and **Rau, H.** *Handbuch der Verkehrsunfall Rekonstruktion*, 1981 (Verlag Information Ambs Gmbh).
41 Wood, D. P. and **Simms, C. K.** Coefficient of friction in pedestrian throw. *Impact, J. ITAI*, 2000, **9**(1), 12–14.

APPENDIX 1

Notation

CG	pedestrian centre of gravity
e	coefficient of restitution
k	pedestrian radius of gyration about CG (m)
M_r	vehicle + pedestrian)/vehicle mass ratio $= (M_v + M_p)/M_v$
R	ground reaction force acting on the pedestrian (N)
S	total pedestrian projection distance (m)
$S_{\text{fall-over}}$	pedestrian projection distance during the fall-over phase (m)
S_{flight}	pedestrian projection distance during the flight phase (m)
S_{impact}	pedestrian projection distance during the impact phase (m)
$S_{\text{slide/roll/bounce}}$	pedestrian projection distance in the slide/roll/bounce phase (m)
V_{col}	vehicle speed just prior to impact (m/s)
V_{cp}	combined vehicle and pedestrian speed just after impact (m/s)
V_{proj}	horizontal projection velocity of the pedestrian after impact (m/s)
μ	coefficient of retardation between the pedestrian and the ground
μ_{braking}	coefficient of vehicle braking

APPENDIX 2

This appendix contains details of the statistical forms and literature sources used to model the input parameters for the Monte Carlo models.

Vehicle mass. A log normal distribution was used to model vehicle mass based on FARS data [**38**]:

Log mean (kg)	7.0723
Log standard deviation (kg)	0.212

Pedestrian mass. Pedestrian mass was modelled using normal distributions derived by Wood and Simms [**10**] and Wood and Walsh [**9**] who used source data from reference [**39**]:

	Adults	Children
Mean (kg)	68.37	30.9
Standard deviation (kg)	16.13	11.7

Pedestrian height. Body height was assumed to be randomly related to mass to account for varying body proportions:

	Adults	Children
Minimum height (m)	1.477	0.87
Maximum height (m)	1.873	1.7

Pedestrian radius of gyration. The radius of gyration is expressed as a normally distributed proportion of body length [**39**]:

Mean k/L	0.23
Standard deviation k/L	0.0175

Pedestrian centre of gravity height. This is expressed as a normally distributed proportion of body length [**39**]:

Mean k/L	0.57
Standard deviation k/L	0.0152

d000001504 08-12-04 13:30:44 Rev 14.05
The Charlesworth Group, Huddersfield 01484 517077

Forward projection impact time. Aldman *et al.* [**19**] measured the contact times during pedestrian impact in 38 tests. The results show a broadly normal distribution:

Mean contact time (s)	0.056
Standard deviation (s)	0.024
Minimum (s)	0.01
Maximum (s)	0.14

Coefficient of restitution. Analysis by Wood and Walsh [**9**] of tests performed by Lucchini and Weissner [**18**] shows a linear dependence of restitution on impact speed

$$e = 0.12 - 0.006 V_{\text{col}} \text{ (m/s)}$$

Coefficient of retardation. Analysis by Wood and Simms [**41**] indicates that the available test data on coefficient of retardation are approximately normally distributed:

Mean	0.561
Standard deviation	0.101